Journal of Power Sources 189 (2009) 411–415

Contents lists available at ScienceDirect

Journal of Power Sources

journal homepage: www.elsevier.com/locate/jpowsour

Short communication

Preparation and electrochemical properties of indium- and sulfur-doped $LiMnO_2$ with orthorhombic structure as cathode materials

Z. Su [a,b], Z.W. Lu [c], X.P. Gao [a,*], P.W. Shen [a], X.J. Liu [c], J.Q. Wang [c]

[a] Institute of New Energy Material Chemistry, Nankai University, Tianjin 300071, China
[b] College of Life Science and Chemistry, Xinjiang Normal University, Urumqi 830054, China
[c] Tianjin Institute of Power Sources, Tianjin 300381, China

ARTICLE INFO

Article history:
Received 8 June 2008
Received in revised form 11 July 2008
Accepted 21 July 2008
Available online 31 July 2008

Keywords:
$LiMnO_2$
Orthorhombic structure
Doping
Cathode materials
Hydrothermal synthesis

ABSTRACT

The indium- and sulfur-doped $LiMnO_2$ samples with orthorhombic structure as cathode materials for Li-ion batteries are synthesized via hydrothermal method. The microstructure and composition of the samples were characterized by X-ray diffraction (XRD), transmission electron microscopy (TEM), inductively coupled plasma atom emission spectroscopy (ICP-AES), and X-ray photoelectron spectroscopy (XPS) analysis. It is shown that these samples with the orthorhombic structure have irregular shapes with a grain size of about 100–200 nm. The electrochemical performance of these samples as cathode materials was studied by galvanostatic method. All doped materials can offer improved cycling stability and high rate discharge ability as compared with the un-doped $Li_{0.99}MnO_2$. Moreover, dual In/S doping can slow down the capacity decay to a great extent, although the transformation to spinel occurs undesirably for all the doped samples during electrochemical cycling.

1. Introduction

The layered $LiMnO_2$ with orthorhombic structure (space group *Pmmn*, hereafter denoted as *o*-$LiMnO_2$), is favourable for lithium insertion and extraction. Usually, *o*-$LiMnO_2$ can be prepared by a conventional solid-state reaction at high temperature under argon or nitrogen [1–3] or by a soft-chemistry route at lower temperature [4–6]. The electrochemical properties of the cathodes are mainly related to crystalline sizes [7,8], which depend on reaction temperature for preparation. Low temperature soft-chemistry routes and moderate synthesis methods are alternative ways to obtain *o*-$LiMnO_2$ cathode materials with fine crystalline sizes and improved electrochemical properties. Although *o*-$LiMnO_2$ materials can offer higher discharge capacities as compared to the sipnel material, it was demonstrated that the rapid decay of the discharge capacity occurred during cycling, due to the irreversible structural transformation from the layered lithium manganese oxides to a spinel structure.

It is shown that element doping in electrode materials is an effective way to improve the electrochemical stabilities. In the past, many efforts were made to enhance the electrochemical stability of *o*-$LiMnO_2$ materials by partial substitution or doping of Mn by Al, Cr, Ni, and Co [9–12]. Meanwhile, sulfur and indium doping was found to be in favour of electrochemical cycling performance in spinel $LiMn_2O_4$ [13–16], overcoming Jahn–Teller distortion [17]. In addition, sulfur doping was also effective to improve the cycling stability of $LiMnO_2$ materials with monoclinic or hexagonal structures [18,19].

In this work, the $LiMnO_2$ with the orthorhombic structure was prepared via hydrothermal method. In addition, a partial indium or sulfur doping, and dual doping in $LiMnO_2$ were investigated. The morphology, microstructure, composition and electrochemical properties of these samples as cathode materials were studied in detail.

2. Experimental

2.1. Preparation and characterization

The starting materials are $LiOH{\cdot}H_2O$ and Mn_2O_3. The mixture of $LiOH{\cdot}H_2O$ (0.30 mol) and Mn_2O_3 (0.01 mol) was put into a Teflon-line autoclave (60 ml), filled with de-ionized water (50 ml). The autoclave was sealed and maintained at 150 °C for 36 h. A brown-black precipitate was collected and washed thoroughly with de-ionized water to eliminate residual alkaline, and was dried in a vacuum box at 105 °C for 12 h to obtain *o*-$LiMnO_2$. Indium-doped $LiMn_{1-y}In_yO_2$ (y = 0.01, 0.02 and 0.03) samples were obtained with the molar ratio Mn/In = 0.99/0.01–0.97/0.03 ($In(NO_3)_3{\cdot}5H_2O$,

* Corresponding author. Tel.: +86 22 23500876; fax: +86 22 23500876.
E-mail address: xpgao@nankai.edu.cn (X.P. Gao).

0378-7753/$ – see front matter © 2008 Elsevier B.V. All rights reserved.
doi:10.1016/j.jpowsour.2008.07.069

Table 1
The chemical composition of the typical samples as measured by ICP

Design formula	ICP results
$LiMnO_2$	$Li_{0.99}MnO_2$
$LiIMn_{0.99}In_{0.01}O_2$	$Li_{1.01}Mn_{0.989}In_{0.011}O_2$
$LiMn_{0.98}In_{0.02}O_2$	$Li_{0.99}Mn_{0.982}In_{0.018}O_2$
$LiMn_{0.97}In_{0.03}O_2$	$Li_1Mn_{0.968}In_{0.032}O_2$
$LiMnO_{1.99}S_{0.01}$	$Li_{0.98}MnO_{1.99}S_{0.01}$
$LiMn_{0.99}In_{0.01}O_{1.99}S_{0.01}$	$Li_{0.99}Mn_{0.988}In_{0.012}O_{1.991}S_{0.009}$

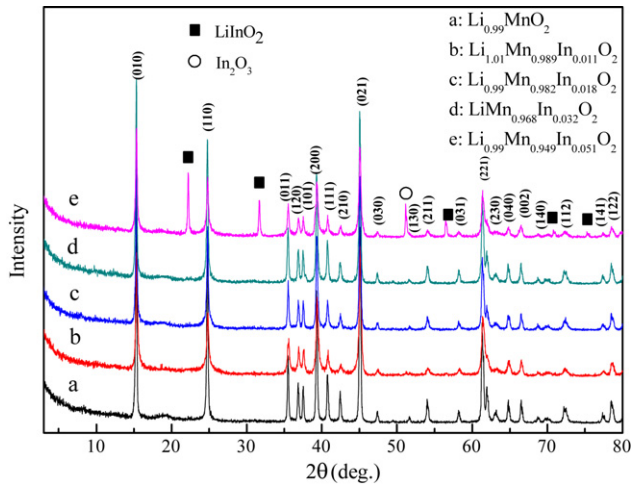

Fig. 1. XRD patterns of the In-doped samples.

0.001–0.03 mol). Sulfur-doped material was prepared in the molar ratio of S/Mn = 0.01/1 ($Na_2S{\cdot}9H_2O$, 0.002 mol). The final indium and sulfur co-doped materials were obtained by the above-mentioned method.

The microstructure of the as-prepared samples was characterized by X-ray diffraction (XRD, Rigaku D/max-2500) with Cu Kα radiation and transmission electron microscope (TEM, FEI Tecnai 20) with an accelerating voltage of 200 kV. Elemental analysis for Li, Mn, In, and S was carried out by using inductively coupled plasma atom emission spectroscopy (ICP-AES, IRIS Advantage) to determine the chemical composition of these materials. The surface chemical state was recorded using an X-ray photoelectron spectroscopy (XPS, PHI-5300 ESCA).

2.2. Electrochemical performance

The working electrode was prepared by compressing a mixture of active materials, acetylene black, and binder (polytetrafluoroethylene, PTFE) in a weight ratio of 75:20:5. Lithium metal was used as the counter and reference electrodes. The electrolyte was $LiPF_6$ (1 M) in a mixture of ethylene carbonate (EC), dimethyl carbonate (DMC), and ethyl methyl carbonate (EMC) with a weight ratio of 1:1:1. All procedures for handing and fabricating the electrochemical cells were performed in an argon-filled glove box. The

Table 2
Lattice parameters of the typical samples after Rietveld refinement

Sample	a (nm)	b (nm)	c (nm)	Cell volume ($\times10^{-3}$ nm^3)
$Li_{0.99}MnO_2$	0.4572	0.5741	0.2803	73.57
$Li_{1.01}Mn_{0.989}In_{0.011}O_2$	0.4571	0.5742	0.2804	73.59
$Li_{0.99}Mn_{0.982}In_{0.018}O_2$	0.4569	0.5743	0.2805	73.60
$Li_1Mn_{0.968}In_{0.032}O_2$	0.4570	0.5744	0.2805	73.63
$Li_{0.98}MnO_{1.99}S_{0.01}$	0.4570	0.5743	0.2805	73.62
$Li_{0.99}Mn_{0.988}In_{0.012}O_{1.991}S_{0.009}$	0.4571	0.5744	0.2806	73.67

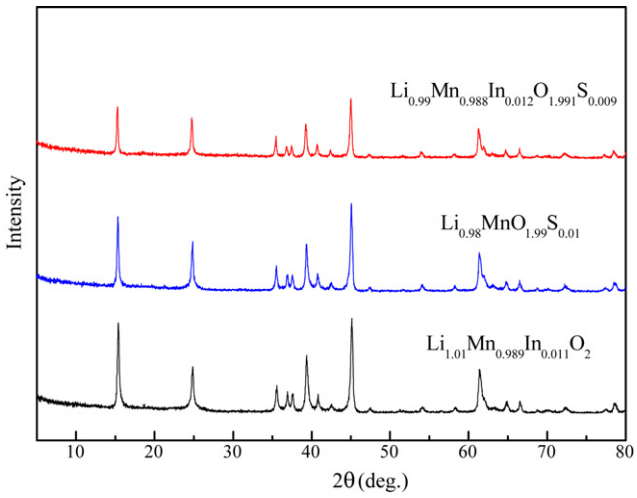

Fig. 2. XRD patterns of the S-doped and In/S-doped samples.

galvanostatic method was used to measure the electrochemical capacity and cycle life of the electrodes at room temperature (25 °C) using a LAND CT2001A instrument. The cut-off potentials for charge and discharge were set between 2.0 and 4.3 V (vs. Li^+/Li).

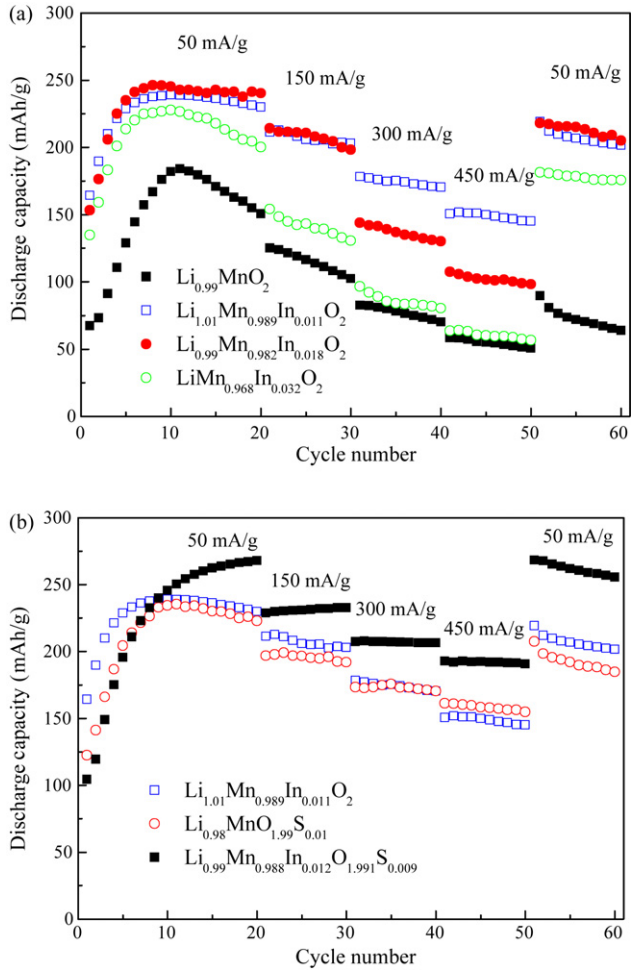

Fig. 3. Cycle performance of the In-doped (a) and In/S-doped (b) samples at various discharge current densities with a charge current of 50 mA/g for all cycles in the potential range between 4.3 and 2 V (vs. Li^+/Li).

3. Results and discussion

The chemical composition of the as-prepared samples, calculated from the results of ICP-AES, is summarized in Table 1. The Li/Mn ratio for all the samples is very close to 1. XRD patterns of the In-doped materials are shown in Fig. 1, their lattice parameters after Rietveld refinement are summarized in Table 2. All XRD peaks, except for the marked peaks of the as-prepared samples, can be assigned to the orthorhombic structure with space group of *Pmmn* (JCPDS 86-0356). In addition, all the samples appear to be well crystalline, based on sharp peaks in XRD patterns. It is notable that increasing the indium concentration in the sample may lead to some impurities. The appearance of $LiInO_2$ (JCPDS 88-1929) and In_2O_3 (JCPDS 89-4595) can be clearly detected for the $Li_{0.99}Mn_{0.949}In_{0.051}O_2$ sample. Therefore, the element-doped concentration in the sample should be kept as low as possible, in order to avoid the formation of impurities. In XRD patterns of S-doped and In/S-doped samples (Fig. 2), all the samples have the same orthorhombic structure without impurities. Thus, the orthorhombic structure is well stabilized even in dual doping with indium and sulfur for the $LiMnO_2$ sample, though the XRD peak intensity is lower, indicating the relatively poor crystallinity of the In/S-doped sample.

In order to compare the cycle stability and high rate discharge ability of these samples, the cycle performance of all the samples at various discharge current densities is presented in Fig. 3. All the samples reach their maximum discharge capacities at about the 10th cycle. It is clear that the cycle performance and high rate discharge ability of the *o*-$Li_{0.99}MnO_2$ sample are poor. The maximum discharge capacity and cycle stability of cathode materials can be greatly improved by indium doping. With increasing the indium-doped concentration, however, the high rate discharge ability turns to decrease. The $Li_{1.01}Mn_{0.989}O_2$ sample is shown to have the optimized electrochemical performance among In-doped samples, including the discharge capacity, cycle stability and high rate discharge ability. The S-doped sample also has improved

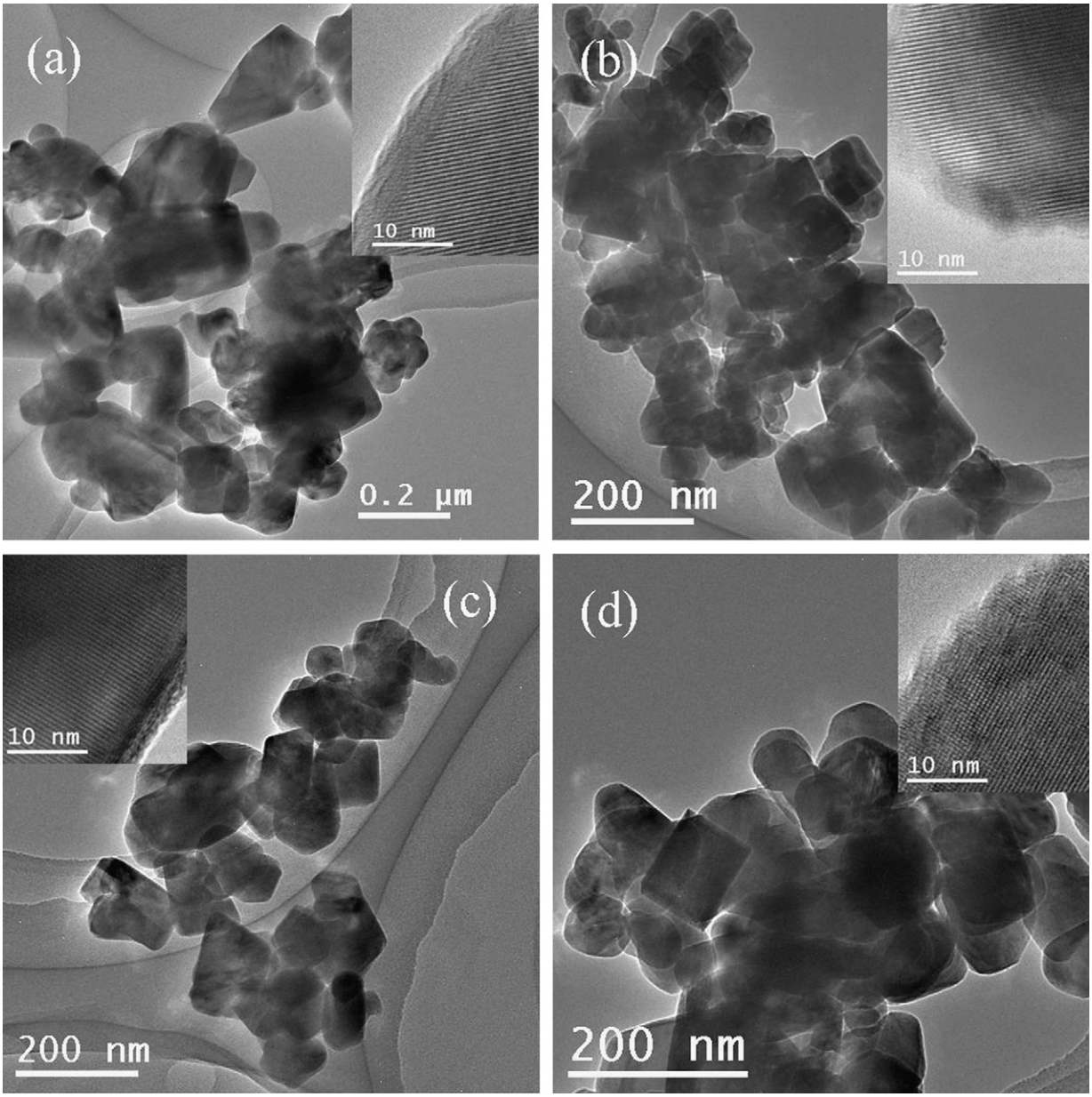

Fig. 4. TEM images of the as-prepared samples. (a) $Li_{0.99}MnO_2$, (b) $Li_{1.01}Mn_{0.989}In_{0.011}O_2$, (c) $Li_{0.98}MnO_{1.99}S_{0.01}$ and (d) $Li_{0.99}Mn_{0.988}In_{0.012}O_{1.991}S_{0.009}$.

electrochemical performance as compared with the *o*-$Li_{0.99}MnO_2$ sample. In particular, the electrochemical performance can be further improved in the dual In/S-doped sample. For example, the $Li_{0.99}Mn_{0.988}In_{0.012}O_{1.991}S_{0.009}$ sample has the maximum discharge capacity of 267.9 mAh/g at the 10th cycle and remains the capacity of 256 mAh/g after 60 cycles at 50 mA/g. Importantly, the high rate discharge ability of the In/S-doped sample is also enhanced as compared with S-doped or In-doped samples.

On the basis of the electrochemical performance, four typical samples ($Li_{0.99}MnO_2$, $Li_{1.01}Mn_{0.989}In_{0.011}O_2$, $Li_{0.98}MnO_{1.99}S_{0.01}$ and $Li_{0.99}Mn_{0.988}In_{0.012}O_{1.991}S_{0.009}$) are selected in further experiments. TEM images of the above four typical samples are illustrated in Fig. 4. It can be seen that these samples, obtained from the hydrothermal route, have irregular shapes with a grain diameter of 100–200 nm. The presence of clear interference fringe in HRTEM images indicates that these grains have a good crystallinity for the $Li_{0.99}MnO_2$, In-doped and S-doped samples. In contrast, the dual In/S-doped sample appears to have a relatively poor crystallinity, in agreement with XRD analysis.

The charge–discharge curves of the four typical samples in the 1st and the 10th cycles are shown in Fig. 5. It is found that all these samples exhibit a long discharge and charge potential plateaus at about 2.8 and 3.5 V (vs. Li^+/Li), respectively, as the characteristics of the layered Li_xMnO_2 materials. The discharge potential plateau at about 4.0 V (vs. Li^+/Li), as usually observed in spinel lithium manganese oxides, is absent. After In or In/S-doping, the initial discharge

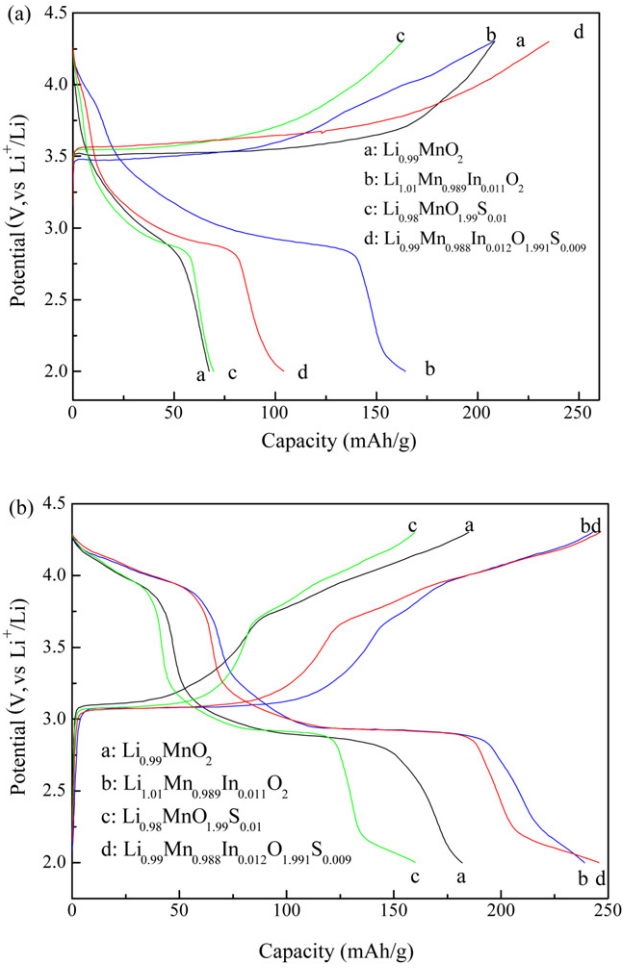

Fig. 5. The charge–discharge curves of the as-prepared samples in the 1st (a) and 10th (b) cycles at 50 mA/g.

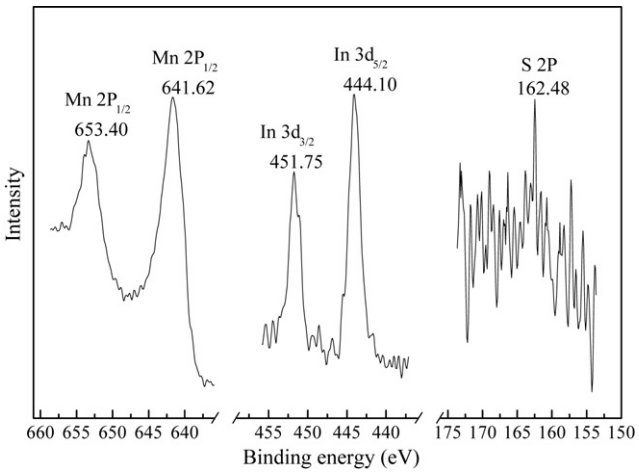

Fig. 6. Mn2p, S2p and In3d core level spectra of the $Li_{0.99}Mn_{0.988}In_{0.012}O_{1.991}S_{0.009}$ sample.

capacity is increased to some extent. After 10 cycles, however, the discharge potential plateau at about 4.0 V (vs. Li^+/Li) appears for all the samples, as shown in Fig. 5b. It means that the partial structural transformation from the layered orthorhombic structure to the spinel structure unavoidably occurs during cycling. The above partial structural transformation was also observed previously in *o*-$LiMnO_2$ cathode materials [2,20,21]. Though the dual In/S-doping in the layered orthorhombic structure can slow down capacity decay, however, it cannot inhibit the partial structural transformation.

Mn2p, S2p and In3d core level spectra of the $Li_{0.99}Mn_{0.988}In_{0.012}O_{1.991}S_{0.009}$ sample are presented in Fig. 6. The characteristic peak (binding energy) of the Mn $2p_{3/2}$ locates at 641.62 eV, almost identical to that in Mn_2O_3 [22], MnOOH [23] and monoclinic $LiMnO_2$ [24], corresponding to the Mn(III) oxidation state. The binding energies of the In $3d_{5/2}$ and S2p are 444.10 and 162.48 eV, respectively, similar to that observed in In_2O_3 [25] and ZnS [26]. Therefore, indium and sulfur exist as the In(III) oxidation state and S(II) reduction state.

In general, element doping with larger ion radius may generate a channel with fast mobility of Li ions. It is known that the ionic radius of In^{3+} (0.081 nm) is larger that that of Mn^{3+} (0.066 nm). In addition, the thermochemical radius of S^{2-} is 0.173 nm [27], larger than O^{2-} ionic radius (0.132 nm). Therefore, the cell volume of all doped samples increases slightly, as compared with the *o*-$Li_{0.99}MnO_2$ sample. Meanwhile, it was reported that dopants with larger ion radius may stabilize the layered structure of monoclinic and orthorhombic $LiMnO_2$ [9–12,28]. The miscibility of dopants into layered $LiMnO_2$ was also considered as the important factor [28]. It is known that $LiInO_2$ compound can exist, similar to $LiMnO_2$, $LiNiO_2$, $LiAlO_2$, $LiCrO_2$, and $LiTiO_2$. Thus, indium may have good miscibility into layered $LiMnO_2$ to maintain cycling stability. In addition, sulfur and oxygen anions have a good replacement mechanism in compounds. Therefore, In/S doping may prevent partially from the structure distortion of layered $LiMnO_2$ during repeated lithium insertion/extraction processes. Even if the transformation to spinel occurs unavoidably for all the doped samples during electrochemical cycling, In/S doping still can slow down the capacity decay to a great extent.

4. Conclusion

The $Li_{0.99}MnO_2$ with the orthorhombic structure can be synthesized via hydrothermal method. The partial In-doped or sulfur-doped, or dual In/S-doped samples are also obtained. It

is shown that the orthorhombic structure is maintained in dual doping with indium and sulfur in the layered sample. All the samples, obtained from the hydrothermal route, have irregular shapes with a grain diameter of 100–200 nm, while maintaining good crystallinity. The electrochemical measurement demonstrates that indium or sulfur doping can improve electrochemical cycle stability and high rate discharge ability. In particular, the dual In/S-doped sample has the optimized electrochemical performance, including the discharge capacity, cycle stability, and high rate discharge ability.

Acknowledgement

This work is supported by the 973 Program (2009CB220100), China.

References

[1] Y.S. Lee, Y.K. Sun, K. Adachi, M. Yoshio, Electrochim. Acta 48 (2003) 1031.
[2] S.H. Wu, M.T. Yu, J. Power Sources 165 (2007) 660.
[3] Y.J. Wei, H. Ehrenberg, N.N. Bramnik, K. Nikolowski, C. Baehtzc, H. Fuess, Solid State Ionics 178 (2007) 253.
[4] A. Manthiram, J. Kim, Chem. Mater. 10 (1998) 2895.
[5] S. Komaba, S.T. Myung, N. Kumagai, T. Kanouchi, K. Oikawa, T. Kamiyama, Solid State Ionics 152 (2002) 311.
[6] J.M. Kim, H.T. Chung, J. Power Sources 115 (2003) 125.
[7] P.G. Bruce, B. Scrosati, J.M. Tarascon, Angew. Chem. Int. Ed. 47 (2008) 2930.
[8] S.H. Ye, J. Lv, X.P. Gao, F. Wu, D.Y. Song, Electrochim. Acta 49 (2004) 1623.
[9] S.T. Myung, S. Komaba, N. Kumagai, J. Electrochem. Soc. 149 (2002) A1349.
[10] Y. Idemoto, D. Shimizu, N. Koura, Electrochemistry 74 (2006) 815.
[11] X.Y. Tu, G.L. Lu, Y.W. Zeng, J. Mater. Sci. Technol. 22 (2006) 45.
[12] X.M. Wu, R.X. Li, S. Chen, Z.Q. He, M.F. Xu, Bull. Mater. Sci. 31 (2008) 109.
[13] Y.K. Sun, Y.S. Lee, M. Yoshio, Mater. Lett. 56 (2002) 418.
[14] M.M. Doeff, J. Hollingsworth, J. Shim, Y.J. Lee, K. Striebel, J.A. Reimer, E.J. Cairns, J. Electrochem. Soc. 150 (2003) A1060.
[15] Y.K. Sun, S.W. Oh, C.S. Yoon, H.J. Bang, J. Prakash, J. Power Sources 161 (2006) 19.
[16] H.W. Liu, C.Q. Feng, H. Tang, L. Song, K.L. Zhang, J. Mater. Sci. 15 (2004) 495.
[17] Y.K. Sun, Y.S. Jeon, H.J. Lee, Electrochem. Solid State Lett. 3 (2000) 7.
[18] S.H. Park, Y.S. Lee, Y.K. Sun, Electrochem. Commun. 5 (2003) 124.
[19] S.T. Lim, D.H. Park, S.H. Lee, S.J. Hwang, Y.S. Yoon, S.G. Kang, Bull. Korean Chem. Soc. 27 (2006) 1310.
[20] J. Molenda, M. Ziemnicki, J. Marzec, W. Zając, M. Molenda, M. Bucko, J. Power Sources 173 (2007) 707.
[21] X.Y. Tu, K.Y. Shu, J. Solid State Electrochem. 12 (2008) 245.
[22] B.R. Strohmeier, D.M. Hercules, J. Phys. Chem. 88 (1984) 4922.
[23] E. Regan, T. Groutso, J.B. Metson, R. Stiner, B. Ammundsen, D. Hassell, P. Picking, Surf. Interface Anal. 27 (1999) 1064.
[24] T.J. Xu, S.H. Ye, Y.L. Wang, H.X. Liang, X.P. Gao, D.Y. Song, Chin. J. Inorg. Chem. 21 (2005) 993.
[25] M. Procop, J. Electron Spectosc. Relat. Phenom. 59 (1992) R1.
[26] C. Battistoni, L. Gastaldi, A. Lapiccirella, G. Mattogno, C. Vticoli, J. Phys. Chem. Solids 47 (1986) 899.
[27] B.J. Tan, K.J. Klabunde, P.M.A. Sherwood, J. Am. Chem. Soc. 113 (1991) 855.
[28] G. Ceder, S.K. Mishra, Electrochem. Solid State Lett. 2 (1999) 550.